
PERGAMON

Journal of the Mechanics and Physics of Solids
49 (2001) 2819–2838

JOURNAL OF THE
MECHANICS AND
PHYSICS OF SOLIDS

www.elsevier.com/locate/jmps

Experimental study of the deformation near a notch tip in copper and copper–beryllium single crystals

W.C. Crone[a,*], T.W. Shield[b]

[a] *Department of Engineering Physics, University of Wisconsin, 1500 Engineering Dr., Madison, WI 53706, USA*

[b] *Department of Aerospace Engineering and Mechanics, University of Minnesota, 110 Union St. SE, Minneapolis, MN 55455, USA*

Received 7 July 2000; received in revised form 3 May 2001; accepted 3 May 2001

Abstract

The plastic deformation around a notch tip within ductile single crystal material was investigated experimentally. Moiré microscopy was used to measure the strain field on the surface of bending samples of Orientation II with a notch on the (0 1 0) plane and its tip along the $[\bar{1}\,0\,1]$ direction. The results of tests conducted on copper and copper–beryllium single crystals are compared to analytical solutions, numerical calculations, and prior experiments on samples of Orientation I with a notch on the (1 0 1) plane and its tip along the $[1\,0\,\bar{1}]$ direction. Distinct sectors with sharp sector boundaries are observed in experiments as were predicted analytically by Rice (Mech. Mater. 6 (1987) 301). However, Rice predicted that both Orientations I and II would give rise to the same sectors. It is found that experimental results for these two orientations differ and neither set of results agree with the analytical solution. In both orientations, the sector boundaries do not exclusively correspond to angles at which slip and kink can occur in these crystallographic orientations. The experiments also lead to the conclusion that some sectors in the deformation field remain elastic even after large amounts of deformation have occurred elsewhere. Based on the optical observations and strain measurements, a stress field is presented for Orientation II.

Keywords: A. Crack tip plasticity; B. Anisotropic material; B. Crystal plasticity; C. Mechanical testing; C. Optical interferometry

* Corresponding author. Tel.: +1-608-262-8384; fax: +1-608-263-7451.
E-mail address: crone@engr.wisc.edu (W.C. Crone).

0022-5096/01/$ - see front matter
PII: S0022-5096(01)00080-1

1. Introduction

Investigation of plastic deformation at a crack tip in a single crystal is important to the development of the understanding of polycrystalline material fracture and single crystal failure. The plastic deformation around a crack tip within a ductile single crystal material produces a plastic field with sectors of deformation and crystallographically dependent radial boundaries. Rice (1987) predicted this type of patchy plastic deformation around a crack tip in metallic single crystals, and this behavior was confirmed experimentally (Tetelman and Robertson, 1963; Cho and Yu, 1991; Shield and Kim, 1994; Shield, 1996; Bastawros and Kim, 1998) and investigated numerically (Rice et al., 1990; Mohan et al., 1992; Cuitino and Ortiz, 1996). Existing analytical and numerical work provides some insight into the behavior of ductile single crystals in the presence of a crack or notch, but the results available do not completely predict the behavior observed in experiments. Additionally, experimental work available on this topic is limited and only begins to elucidate the complex behavior that occurs at a crack or notch in a ductile single crystal. The research discussed below involves a detailed experimental exploration of the relationship between orientation and the plastic deformation that develops at a notch. The results for one crystallographic orientation are compared and contrasted to existing analytical and numerical work.

In elastic perfectly plastic material models, it is assumed that when the critical shear stress is reached slip can occur and the material can undergo plastic deformation. A surface can be described in stress space that identifies the stress conditions under which yield is reached for a material. For an anisotropic material in plane strain, Rice (1973) showed that the yield surface can be constructed in $(\sigma_{11}-\sigma_{22})/2$ vs. σ_{12} stress space. The projected shape of the yield surface is dependent on the crystallographic orientation being considered as well as the active slip systems allowed by crystallography. The yield surface for a particular crystallographic orientation of an FCC material is shown plotted in this stress space in Fig. 1.

Two crystallographic orientations are considered in this research. Orientation I will be defined as the orientation containing a crack (theory) or notch (experiment) on the $(1\,0\,1)$ plane and its tip along the $[1\,0\,\bar{1}]$ direction. This orientation was investigated experimentally by Shield (1996) and Shield and Kim (1994). Orientation II will be defined as the orientation containing a crack or notch on the $(0\,1\,0)$ plane and its tip along the $[\bar{1}\,0\,1]$ direction. Experimental results for this orientation are presented below. The plane of observation is the same for these two orientations and the crack or notch is rotated by 90°. Both orientations were analytically investigated by Rice (1987).

Consider Fig. 1 where three families of slip plane traces are shown in the (x_1,x_2) plane relative to the crack orientation. For the family of dashed lines parallel to the crack and the x_1 axis, the effective slip is in the direction $[1\,0\,1]$. This slip is produced by simultaneous slip on the planes $(1\,\bar{1}\,\bar{1})$ and $(1\,\bar{1}\,1)$. These pairs of slip planes are grouped as a single slip plane strain system for this discussion. The effective slip in the $[1\,0\,1]$ direction corresponds to the line segments BC and FE on the yield surface of Fig. 1. The slip systems in each sample are identified by the angle, θ, that the slip plane traces make with the x_1 axis on the specimen surface.

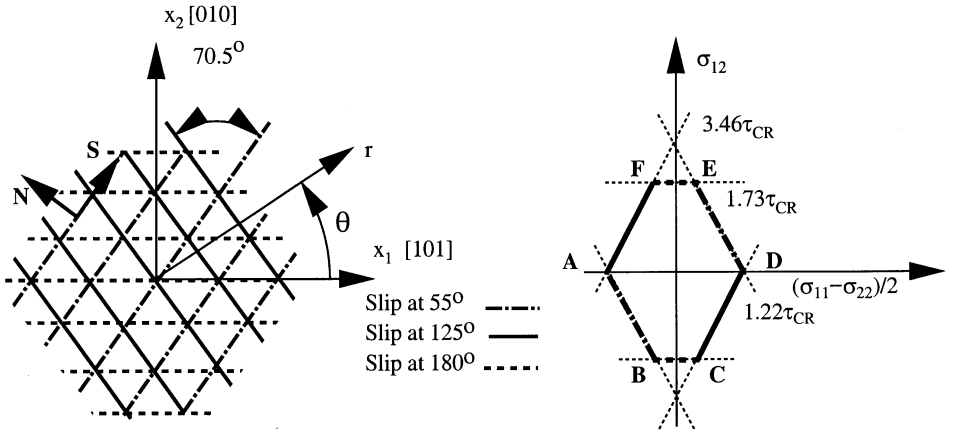

Fig. 1. The diagram on the left shows the orientation of slip plane traces on a specimen surface for an FCC material of Orientation II. The slip plane trace angles depicted occur at 55°, 125°, and 180° from the x_1 axis. The slip systems correspond to lines on the yield surface. For example, the slip in the [1 0 1] direction (shown as dashed lines) at 180° from the x_1 axis corresponds to the line segments BC and FE on the yield surface shown on the right. Adapted from Rice (1987).

Rice (1987) developed a plane strain slip line theory that allowed the construction of a plastic solution for an anisotropic material. He used this theory to produce solutions for cracks in an anisotropic body using a rigid/plastic homogeneous incompressible material. It was assumed that all the material around the crack tip is at yield and that the loading is proportional. The solution must also comply with the principle of maximum plastic work.

Combining conditions for a bounded near-tip stress state with equilibrium allows derivation of an analytical solution with constant stress sectors. For all values of θ except the four special values where $\partial r/\partial \boldsymbol{x}$ aligns with $\boldsymbol{N}$ or $\boldsymbol{S}$ (where $\boldsymbol{S}$ is a unit vector in the slip direction and $\boldsymbol{N}$ is the slip plane normal), it is required that

$$\lim_{r\to 0}\left[\frac{\partial \sigma_{11}}{\partial \theta}\right] + \lim_{r\to 0}\left[\frac{\partial \sigma_{22}}{\partial \theta}\right] = 0. \tag{1}$$

For all bounded near-tip stress states consistent with equilibrium, this implies that

$$\lim_{r\to 0}\left[\frac{\partial \sigma_{\alpha\beta}}{\partial \theta}\right] = 0, \tag{2}$$

where stress is given by $\sigma_{\alpha\beta}$ with Greek indices ranging over 1 and 2, following summation convention. Eq. (2) indicates that as $r \to 0$, the stress state in angular sectors which are at yield must be constant. Thus, the solution contains only constant stress sectors. Changes from one stress sector to another can only occur at angles of $\boldsymbol{S}$ and $\boldsymbol{N}$. Because it is assumed that yield occurs at all angles about the tip (i.e., a fully plastic field), it is required that the sectors be connected to each other by straight lines on the yield surface.

A simple solution with a fully plastic field at one stress state might be suggested, but the boundary conditions of the crack problem cannot be met if $\sigma_{\alpha\beta}$ is constant for

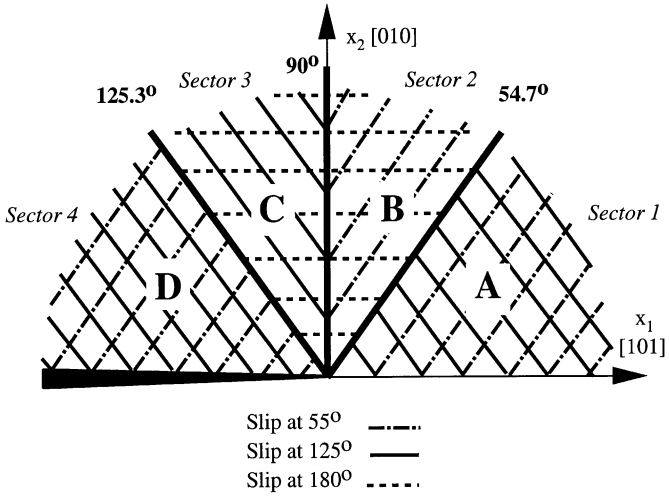

Fig. 2. Rice's (1987) analytical perfectly plastic solution for Orientation II. The thick lines delineate the sector boundary angles. The thin and broken lines indicate the slip plane traces that correspond to the two slip systems available at the corner of the yield surface within each sector. The letters labeling each stress sector correspond to corners of the yield surface shown in Fig. 1. Adapted from Rice (1987).

all θ. The inclusion of discontinuous changes in stress allows the construction of valid solutions satisfying all of the boundary conditions. According to Rice's (1987) theory, a discontinuity can only occur across lines in the direction of $\boldsymbol{S}$ or $\boldsymbol{N}$, and the stress state must change from a corner to a neighboring corner of the yield surface. Rice (1987) notes that if the stress state does not change from a corner to another corner of the yield surface then another jump is not possible unless a sector subtends exactly 90°.

When the stress state changes from one corner to another corner on the yield surface, the discontinuities across lines in the direction of $\boldsymbol{S}$ and $\boldsymbol{N}$ must satisfy the jump condition

$$\|\tfrac{1}{2}(\sigma_{11}+\sigma_{22})\| = -\|L\|, \tag{3}$$

where L is the distance between adjacent corners. Boundary conditions, such as $\sigma_{22}=0$ on the crack face, are then used to construct the solution. Successive calculations can then be made to progress from one sector to another moving from corner to corner on the yield surface.

Rice's (1987) analytical solution for Orientation II is shown in Fig. 2. This solution exhibits constant stress sectors and sector boundary angle discontinuities at 54.7°, 90°, and 125.3°. The four sectors in this solution have active slip systems corresponding to the corners of the yield surface A, B, C, and D in the $+\theta$ half plane. The requirement that all sectors be at a corner of the yield surface implies that double slip (double meaning two in terms of plane strain slip systems, four in terms of 3-D slip systems) occurs in each sector.

Table 1
Analytical and experimental values of sector boundary angles are shown for Orientation I. Results are presented for the analytical solution from Rice (1987), experimental findings for Cu FCC material from Shield (1996), and experimental findings for FeSi BCC material from Shield and Kim (1994)

Sector boundary	Analytical	Experimental	
	Rice (1987) (deg)	FeSi BCC Shield and Kim (1994) (deg)	Cu FCC Shield (1996) (deg)
1–2	54.7	35	43
2–3	90.0	65	62
3–4	125.3	110	100

Zhang and Huang (1994) derived two additional solutions to the one proposed by Rice (1987) by admitting 90° sectors that lie along a flat of the yield surface. Rice's solution contains four sectors, while the two additional solutions contain three sectors. Although these solutions demonstrate nonuniqueness, they bear no resemblance to the experimental results.

The above discussion has been limited to perfectly plastic anisotropic materials, which is relevant for low hardening rate materials. Other analytical results are presented by Saeedvafa and Rice (1989) where Taylor power-law hardening is included in an HRR type solution for the problem of a crack in an anisotropic material. Their solution for the Orientation II contains 7 or more sectors (depending on the value of the hardening exponent, N, where an infinite value of N is the perfectly plastic case) and traverses the yield surface shown in Fig. 1 from flat FA towards corner D counterclockwise in the $+\theta$ half plane. The locations of the sector boundary angles vary with the hardness.

Based on the theory summarized above, it is clear that stress discontinuities are allowed only along slip planes (in the direction of $\boldsymbol{S}$) and normal to slip planes as kink-like shear (in the direction of $\boldsymbol{N}$). In practice, the slip plane traces that intersect with the plane of observation correspond to persistent strain localization bands observed on the surface of experimental samples. The observable persistent strain localizations form in ductile materials such as copper as either slip bands or kink-like shear bands. Slip bands are formed by edge dislocations in the slip plane, and kink bands are formed by two opposing edge dislocations. The experimentally measured slip band angles discussed below are equated to theoretically determined slip plane trace angles.

Two particularly relevant experimental studies have been conducted which can be directly compared to the analytical solutions discussed above. Orientation I was investigated experimentally by Shield (1996) in FCC copper single crystal material and by Shield and Kim (1994) in BCC iron–silicon single crystal material. Their experimental results are compared to Rice's (1987) analytical results in Table 1. The experiments displayed a strain field made up of three constant strain sectors and a sector which has approximately a $1/r$ radial dependence. Narrow transition regions between sectors are observed where the strain varies rapidly. Although no difference in the sector angles is predicted in Rice's (1987) theory for BCC and FCC materials because of the assumed interchangeability of $\boldsymbol{S}$ and $\boldsymbol{N}$, sector boundary angles observed in experiments differ between the BCC and FCC results. Interchangeability of $\boldsymbol{S}$ and $\boldsymbol{N}$ also allows

Table 2
Experimental sector boundary angles for samples C4, C8, C9, and CB1 of Orientation II are compared to the analytical solution from Rice (1987), the numerical solution of Mohan et al. (1992), and the numerical solution of Cuitino and Ortiz (1996). The origin used for measurements was 50 μm ahead of the notch tip

Sector boundary	Experimental	Analytical	Numerical	
	C4, C8, C9, CB1 (deg)	Rice (1987) (deg)	Mohan, Ortiz and Shih (1992) (deg)	Cuitino and Ortiz (1996) (deg)
1–2	50–54	54.7	40	45
2–3	65–68	90	70	60
3–4	83–89	125.3	112	100
4–5	105–110		130	135
5–6	150			

Rice's analytical solution to be applied to both Orientations I and II where the plane of observation is the same and the notch is rotated by 90°.

In addition to the analytical and experimental work discussed above, numerical investigation has been conducted on this problem. Recent numerical work published on this topic by Cuitino and Ortiz (1996) used a three-dimensional finite element model for the specific geometry of the notched four-point-bend samples used in the experiments of Shield and Kim (1994), Shield (1996), and the current research. One orientation was investigated with this model and there were six elements in the thickness direction. Cuitino and Ortiz (1996) found a dependence of the near-tip field on hardening, differences between the surface and interior fields, and the shift from double slip to triple slip (slip on three slip systems in the same region) with hardening. Mohan et al. (1992) used an applied K_I field while Cuitino and Ortiz (1996) used four-point-bend loading. Both models display similar results to the analytical work described above although significant differences in the sector boundary angles are observed as shown in Table 2. Cuitino and Ortiz (1996) conclude that the problem under consideration is not plane strain because of differences between the interior and surface fields as well as a pattern of slip activity which produces significant out of plane strains. Cuitino and Ortiz also predict clear differences in the sector locations on the yield surface with different hardening coefficients.

In order to answer the questions left open in the previous research, experiments were conducted on single crystal Cu and CuBe samples of Orientation II. Comparisons of the sector boundary angles and the stress state of sectors will be made between the new experiential findings for Orientation II, existing experimental results for Orientation I, analytical solutions, and numerical calculations. Issues such as interchangeability of $\boldsymbol{S}$ and $\boldsymbol{N}$, the link between sector boundary angles and directions of $\boldsymbol{S}$ and $\boldsymbol{N}$, assumption of a fully plastic field, and the plane strain nature of the problem are addressed.

2. Experimental procedure

Single crystals of copper and copper–beryllium were grown with the Bridgman technique using a Crystalox, LTD vertical Bridgman system. The Cu material was from the

same crystal as used by Shield (1996). The CuBe crystal was grown from Cu-1.8 wt% Be alloy 125 with a melt temperature of 1350°C, a growth temperature of 1260°C, and a translation rate of 10 mm/hr with two solidification passes (Crone, 2000).

Electrical discharge machining with a Mitsubishi Model DWC90C C-Series Electrical Discharge Machine EDM was used for all cutting operations. X-ray microdiffraction with a Siemens HI-STAR Area Detector System using General Area Detector Diffraction Software was used for crystallographic orientation of the material. The sample preparation involved electrical discharge machining to cut the basic geometery and skim cut the observation surfaces. These operations were followed by heat treatment of the sample in an argon atmosphere for annealing or hardening, chemical etching with a 50% nitric acid solution to clean the material surface, fine wire EDM cutting to create the notch, mechanical polishing to provide an optically reflective surface, and photolithographic application of a 5 μm (200 lines/mm) photoresist grating for moiré microscopy.

The four-point-bend specimens used in testing were 6.35 mm square and have a total length of 5.1 cm with a central single crystal section of approximately 2 cm. The 100–200 μm width notch is cut to a depth of approximately 2.5 mm. Extensions of polycrystalline Cu were attached with epoxy. The copper specimens used in this research are prefaced with 'C' and identified as C4, C8, and C9. The three Cu specimens were duplicate samples loaded to different final displacement levels. The copper–beryllium specimens are prefaced with 'CB' and identified as CB1, CB5, and CB7. The three CuBe specimens were heat treated to produce different hardness levels.

Mechanical testing and data collection through optical and interferometric methods were conducted on three copper single crystal samples and three copper–beryllium single crystal samples of Orientation II. An Instron 4502 Universal Testing Machine was used to apply load to the four-point-bend samples. Load was applied to the specimen through 6.35 mm hardened steel dowels in a four-point-bend jig. The distance between the two sets of dowels was 2.54 and 3.81 cm. The test control and data collection for load and crosshead displacement were performed with a 486 class computer via an IEEE-488 interface board.

In ductile single crystal copper, persistent strain localization bands develop on the surface of the material with plastic deformation. These bands can be observed optically and provide a significant amount of information about the active slip systems within a sector and the sector boundary angles. Optical observation during testing was conducted using a macro lens mounted on a CCD camera. Post-test optical images were obtained with a Nikon microscope equipped with differential interference contrast (DIC) objectives. This technique yields an image with a shadow relief related to the gradient of the optical path difference, which shows small differences in the tilt of the surface as different colors.

Copper–beryllium (CuBe 1.8–2.0 wt%) specimens were used in the moiré experiments. This material was chosen because its structure is similar to pure copper and it is hardenable with heat treatment. The higher hardening rate inhibits the formation of persistent strain localization bands and produces more uniform deformations which provides more accurate moiré microscopy results. Additionally, by using different temperature and heat treatment time in the aging process this material can be used to investigate the effect of hardness on the strain field that develops at the notch tip. The

Table 3
Vickers hardness values are given for oriented CuBe single crystals. Hardness measurements were conducted on [1 1 0] faces. The CuBe samples were solution treated at 790°C for 0.5 h prior to precipitation treatment

Sample	Precipitation treatment	Vickers hardness (kg/mm^2)
C9	None	87
CB1	None	134
CB5	0.5 h at 200°C	155
CB7	1 h at 200°C	167

three CuBe samples tested for Orientation II were heat treated using precipitation times ranging from 0.5 to 1.5 h and temperatures between 200°C and 315°C to produce a range of hardness values. For comparison with the hardness values shown in Table 3, tests on a pure copper single crystal resulted in a hardness level of 87 kg/mm^2.

Moiré microscopy, an optical interference technique, was used to measure the surface components of Almansi strain. The moiré microscope creates interference by illuminating the specimen grating with two coherent beams produced with a He–Ne laser. Interference of a pair of diffracted beams from the specimen grating creates fringes that were analyzed to produce measurements of the in-plane strain field (Shield and Kim, 1991). The strain measure used in the analysis of the moiré fringes is the Almansi strain. Almansi strain, which is a measure of strain in the current configuration, is given by

$$\varepsilon = \tfrac{1}{2}[\boldsymbol{I} - (\boldsymbol{F} \cdot \boldsymbol{F}^{\mathrm{T}})^{-1}], \tag{4}$$

where $\boldsymbol{F}$ is the deformation gradient and $\boldsymbol{I}$ is the identity tensor. It is independent of the reference grating orientation and properly invariant to rigid body motions if an initially orthogonal specimen grating is used. The moiré microscope was placed on an elevator platform on the Instron testing machine in order to take data in situ without unloading the sample. Loading was halted during testing so that moiré fringe images could be captured. Full field strain maps were created from the collected data after testing was completed.

3. Results

Samples were loaded in four-point-bending to the predetermined displacement levels shown in Fig. 3. Loading was paused periodically to collect data which is indicated by the small unloading portions of these curves. Displacement was measured from cross head motion. The ordinate is given in terms of the nominal isotropic stress intensity factor, K_{I}, calculated for the notched four-point-bend specimen geometry assuming a sharp crack. The solid circles in Fig. 3 indicate the load levels at which strain data obtained by moiré microscopy is reported. For CuBe samples with minimal heat treatment, the effect of hardening is minor at these load levels and comparisons can be made with the elastic perfectly plastic theory.

The formation of persistent strain localization bands was observed optically on the sample surface during testing and after unloading as shown in Fig. 4. The persistent

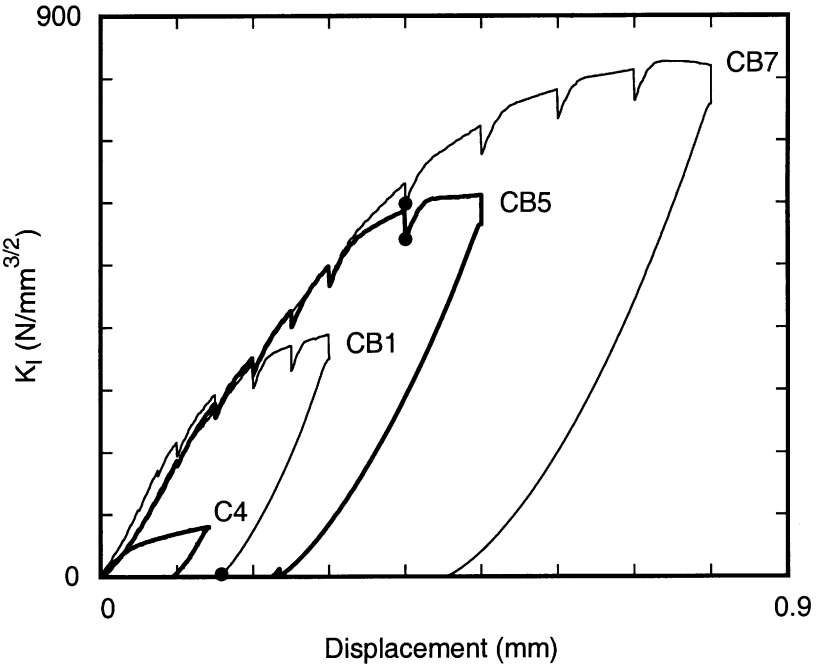

Fig. 3. Loading curves for Cu and CuBe samples of Orientation II are plotted. The solid circle symbols indicate the load level at which moiré strain data is reported for each sample. Displacement values are positive in compression.

strain localization bands that developed on the surface of Cu samples provided information about the active slip systems within a sector and delineated the sector boundary angles. Sector boundaries are identified within the annulus of validity as shown in Fig. 5. The sectors identified in this manner correspond to the sectors of plastic deformation observed around the notch tip with moiré microscopy. Each persistent strain localization band (or persistent strain localization band angle in the x_1–x_2 plane) occurs from simultaneous slip on two systems. The appearance of persistent strain localization bands demonstrates activity on a slip system, but the lack of these bands does not preclude activity. Although the persistent strain localization bands do not provide quantitative information about the amount of deformation, they can be used to determine where plastic deformation occurs first, the active slip systems, the evolution of the deformation, and the structure of the plastic field at the notch tip.

The theoretical slip plane trace angle between the slip plane trace and the x_1 axis is of particular interest for comparison to the persistent strain localization band angles observed in experiments. Because FCC copper slips on $\{1\,1\,1\}$ planes in $\langle 1\,1\,0\rangle$ directions, the slip plane trace angles are 55°, 125°, and 180°. The related kink-like shear trace angles are 35°, 90°, and 145° from the x_1 axis. Because the crystallographic orientation of the sample was known, it was confirmed that all of the persistent strain localization bands observed on the sample surface were at orientations corresponding

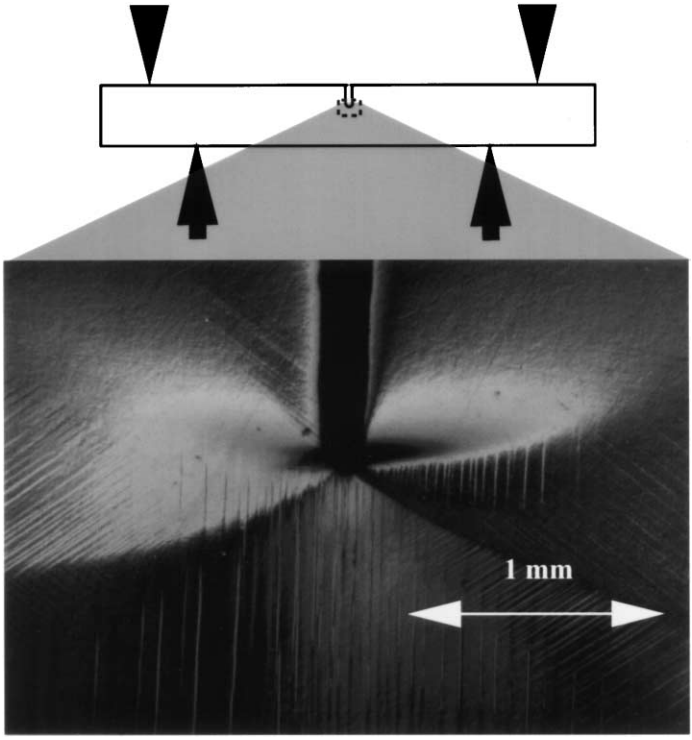

Fig. 4. The optical micrograph was taken using a DIC microscope of sample C8 with Orientation II after deformation. The notch is coming in from the top. The lines in the sectors emanating from the notch tip are slip lines. Changes in color/shade indicate small changes in surface tilt. The black regions very near the tip are regions with larger out of plane deformation and thus larger tilt. The field of view is 2.7 by 1.8 mm.

to the plane strain slip systems available. Thus, all of the persistent strain localization bands observed are categorized as slip bands.

Slip bands occurred initially in one sector and additional slip bands developed at further distances from the notch tip in the same sector with continued loading. Both the length of the bands and the number of bands increased until the sector was filled. Sector boundaries can be easily distinguished by a change in the orientation of the slip bands or a transition to a region containing no observable persistent strain localization bands. Initially only one slip system was observed within a sector. Double slip and triple slip occurred with additional loading in some sectors and in small regions. No additional sectors appeared in low strain regions with more severe deformation (Crone, 1998).

Because of the observable persistent strain localization bands, sector boundary angles can be identified in Cu specimens with optical microscopy. Additionally, the angles of the persistent strain localization bands can be correlated to the allowable slip plane trace angles which correspond to particular portions of the yield surface and therefore particular stress states. In some cases, the number of possible stress states for a sector

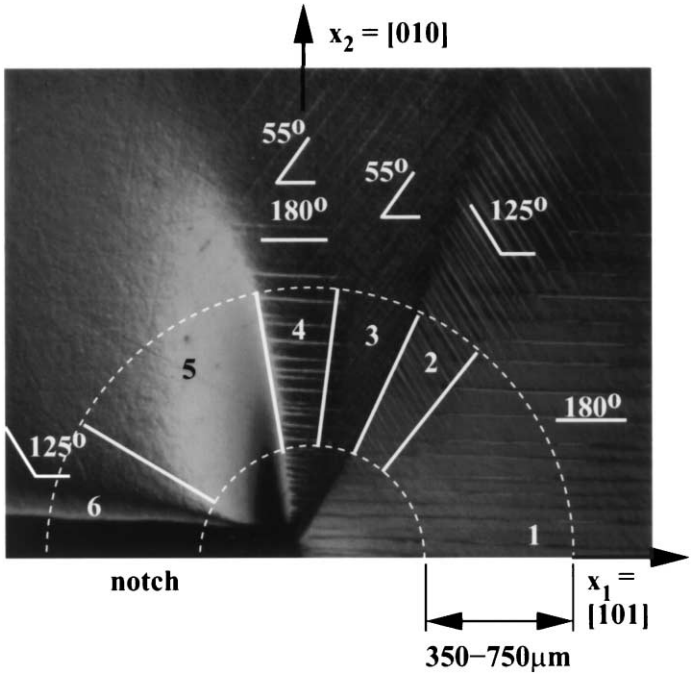

Fig. 5. The $+\theta$ half plane for the same optical micrograph from Fig. 4 is shown here rotated by 90°. The annulus of validity where angular measures are taken is shown by the white half circles. The orientation of the slip lines observed in each sector is also indicated.

can be reduced to only a few options. In Orientation II, for instance, Sector 4 (counting sectors counterclockwise from x_1 in the $+\theta$ half plane) displays slip bands at 55° and 180° from the x_1 axis as shown in Fig. 5. This reduces the possible stress states to corners B and E of the yield surface because these locations are the only points on the yield surface where both of these slip systems can be active simultaneously. Strain measurement is required to determine the slip direction that has the same sign as the stress, thus identifying a region of the yield surface to further reduce the options in the possible stress states for each sector.

The moiré data collected from CuBe samples during loading provides full field in-plane strain measures for a region of the specimen surface surrounding the notch tip as shown in Fig. 6. Excellent correlation is found between the observed persistent slip band angles in Cu samples and the angle of maximum shear strain calculated from the moiré data taken on CuBe samples. This lends weight to the use of slip band observations as an experimental tool to identify the primary source of deformation within a sector. Analysis of the strain data also indicates that deformation is sometimes occurring on more than one slip plane within a sector although slip bands are only observed in association with one of these planes.

For quantitative assessment, strain data has been taken from annular segments of the full field strain maps. The annulus is chosen following Shield and Kim (1994) to avoid

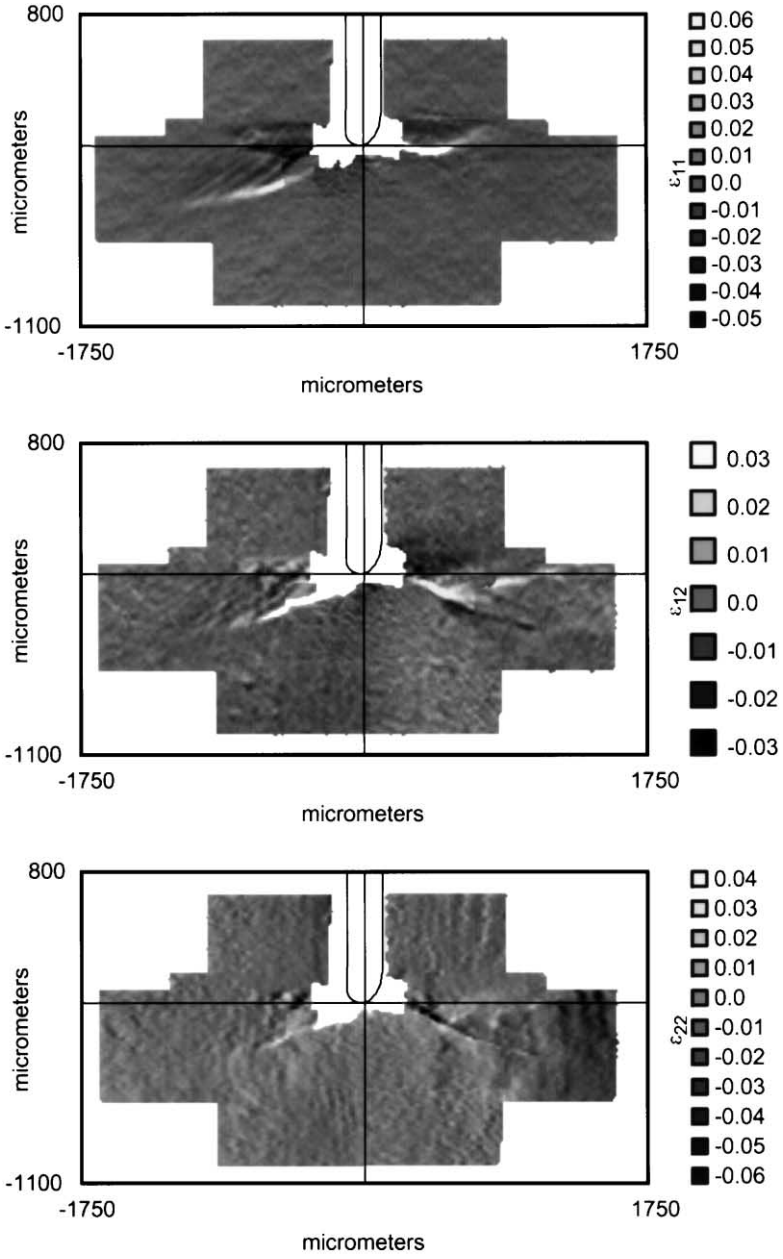

Fig. 6. Strain maps for sample CB1 of Orientation II are shown after deformation (see Fig. 3). The top image shows ε_{11}, the middle image shows ε_{12}, and the bottom image shows ε_{22}. The notch is shown coming down from the top.

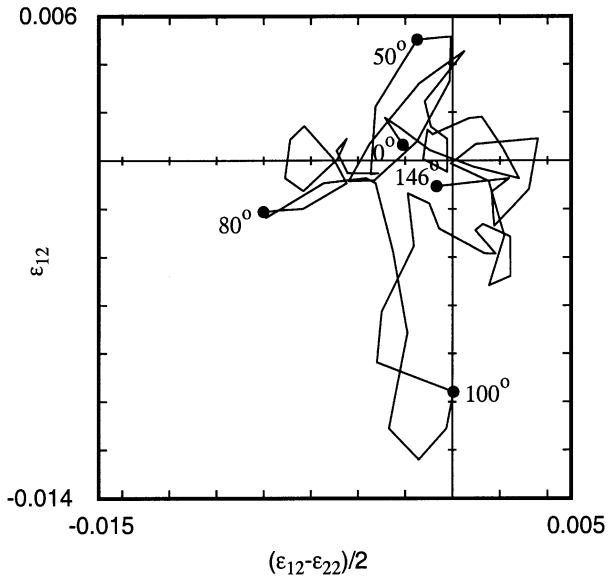

Fig. 7. The strain components are plotted in strain space for sample CB5 of Orientation II at a radius of 350 μm averaged radially over 60 μm. The numerical values identified on the plot indicate the angle from the x_1 axis at which the strain data was measured.

material close to the notch which is dominated by the notch geometry and material in the far field where the proximity of the specimen boundaries has an impact. If a radius for the annulus is taken as 350 μm and a radial average is performed over 60 μm, this data can be plotted in strain space; ε_{12} versus $(\varepsilon_{11} - \varepsilon_{22})/2$. Such a plot is shown in Fig. 7. From the principle of maximum plastic work, it follows that the work done is maximum only if the incremental plastic strain vector is normal to the yield surface in stress space. If it is assumed that the direction of the vector from the origin to the current strain state in the strain space plots corresponds to the direction of a strain increment, then the principle of maximum plastic work allows correlation between the strain state and stress space. Additionally, elastic sectors can also be hypothesized from the measured strains. Some regions are speculated to remain elastic even after large amounts of deformation have occurred elsewhere.

Using the strain measurements presented above, further refinements of the stress state estimate can be made to the results derived from observations of persistent strain localization bands. A six sector solution is derived from the experimental results for Orientation II. Each sector is labeled in Fig. 8 according to which corners of the yield surface are possible given the experimental evidence. How these results were deduced is explained next.

It is noted that slip bands at 180° occur in the copper samples ahead of the notch even though σ_{12} must be zero on $\theta = 0$ from symmetry. Using the assumptions of Rice (1987), it is required that plastic sectors be constant stress sectors. Therefore if σ_{12} is zero at $\theta = 0$ then it follows that σ_{12} must be zero in the entire sector ahead of

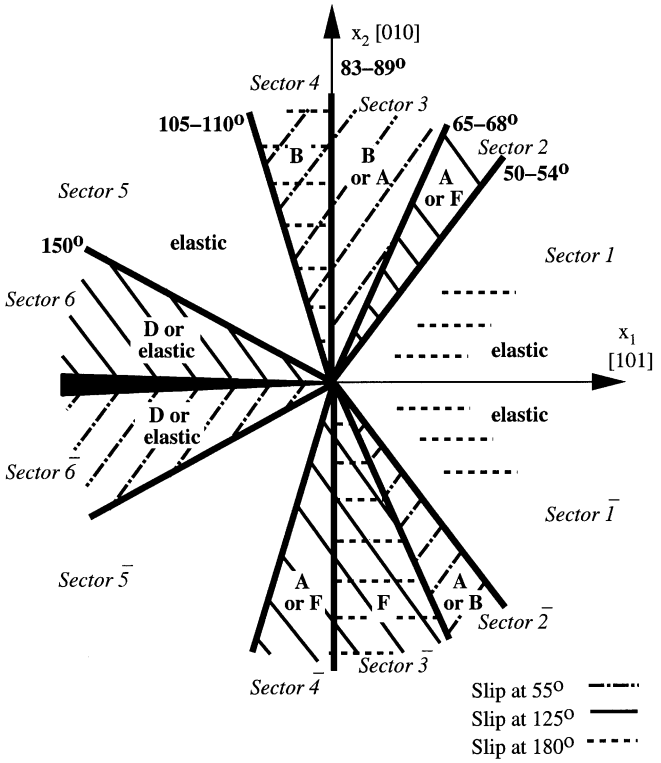

Fig. 8. Identification of stress states near a notch/crack tip for Orientation II, derived from experimental results. The thick lines delineate the sector boundary angles. The thin and broken lines indicate the slip plane traces that correspond to the slip bands observed experimentally. The letters identify each sector's deduced correspondence to corners of the yield surface shown in Fig. 1.

the crack. Following this line of reasoning, the slip bands observed at 180° in Fig. 4 would be impossible. However, the experiments show clearly observable slip activity ahead of the notch even though the strains measured in this region are fairly low. If the results of Saeedvafa and Rice (1989) are considered, then the reason for this activity becomes more obvious. Even a low level of hardening significantly affects the value of σ_{12} very near $\theta = 0$. Although single crystal Cu is a low hardening material, slip bands are observed in the vicinity of $\theta = 0$ because of this effect. Additionally, nonzero shear stress near x_1 is also promoted by the finite notch geometry. For comparison to the perfectly plastic sharp crack solutions, the slip bands at 180° will be taken as an artifact and the sector ahead of the notch in Orientation II will be identified as an elastic sector.

The stress state within plastic sectors in Fig. 8 can be identified by considering both the persistent strain localization bands present and the value of the strains measured. Sectors are numbered in the $+\theta$ half plane starting with Sector 1 ahead of the crack tip and counting counterclockwise to the crack face. The slip bands at 125° indicate a

stress state at corners A, F, C, or D of the yield surface for Sector 2, but the options are reduced to A or F because of the negative value of $(\varepsilon_{11} - \varepsilon_{22})/2$ in this region. Similarly, in Sector 3 stress states at A, B, E, or F are indicated by the slip bands at 55° but the options are reduced to A or B with the strain measurements. Sector 4 can be more accurately identified because of slip bands observed at both 55° and 180° which allows only the possibilities of B or E. Because the values of both $(\varepsilon_{11} - \varepsilon_{22})/2$ and ε_{12} are negative in this region the stress state must be at B. Sector 5 is concluded to be elastic because of the lack of slip bands and the low strain measurements in this region. Sector 6 has low strain measurements but some slip is observed at 125° and the value of $(\varepsilon_{11} - \varepsilon_{22})/2$ is positive and the shear strain must be zero at the notch face, so this sector is either elastic or at stress state D on the yield surface. To summarize, Orientation II is concluded to have the following stress state progression from 0° to 180°: elastic → A or F → A or B → B → elastic → D or elastic. If Sectors 3 and 4 are both B then the six sectors collapse to five sectors.

As Fig. 4 indicates, sector boundary angles observed in the experiments are symmetric across the plane of the notch, but the stress states within sectors in the $-\theta$ half plane do not follow directly from the $+\theta$ half plane. Using the same methodology described above, Orientation II is concluded to have the following stress state progression from 0° to −180°: elastic → A or B → F → A or F → elastic → D or elastic. If Sectors $\bar{3}$ and $\bar{4}$ (counting clockwise from x_1 in the $-\theta$ half plane) are both F then the six sectors collapse to five sectors. Sectors are numbered in the $-\theta$ half plane starting with Sector $\bar{1}$ ahead of the crack tip and counting counterclockwise to the crack face.

Further analysis of the results shown in Fig. 8 allows the stress state possibilities to be reduced. If Rice's (1987) requirement that the stress state must change from corner to neighboring corner of the yield surface is held, then only some stress state progressions are possible candidates. In the $+\theta$ half plane for instance, it is possible to have elastic → F → A → B → elastic → D or elastic; or elastic → A → B → B → elastic → D or elastic; or elastic → A → A → B → elastic → D or elastic. In the $-\theta$ half plane, it is possible to have elastic → A → F → A → elastic → D or elastic; or elastic → A → F → F → elastic → D or elastic.

4. Comparison to analytical solutions

Comparison with the analytical solution raises some issues that are not easily resolved. In Rice's (1987) theory, only sector boundary angles associated with ***S*** and ***N*** directions are allowed between plastic sectors, additionally the angle of slip or kink must be associated with the side of the yield surface connecting the two stress states. The experimentally observed sector boundary angles 2-3 and 3-4 in Fig. 8 are in conflict with these conditions. Sector boundary angle 2-3 falls between two plastic sectors which contain persistent strain localization bands and large strains, however, there is no slip or kink angle near 65–68° where the boundary occurs. Another issue arises with sector boundary angle 3-4. This boundary falls between Sector 3 which has a stress state of A or B, and Sector 4 which has a stress state of B. However, slip on the line of the yield surface connecting A and B occurs at 54.7° and kink at 144.7°, thus a

Table 4
Experimental sector boundary angles for copper samples. The origin used for measurements was 50 μm ahead of notch tip

Sector boundary	Orientation I (1 0 1) Plane [1 0 $\bar{1}$] Tip (deg)	Orientation II (0 1 0) Plane [1 0 $\bar{1}$] Direction (deg)
1–2	35–40	50–54
2–3	54–59	65–68
3–4	111–116	83–89
4–5	138	105–110
5–6		150

sector boundary angle near 90° cannot separate an A sector from a B sector. Further analytical work by Drugan (2001) and Crone and Drugan (2001) is being conducted in an attempt to resolve some of these issues and develop more predictive solutions.

Table 2 summarizes the sector boundary angle results of experimental, analytical, and numerical work on Orientation II. Comparison between the experimental and analytical findings shows some discrepancies. Six sectors were identified from the experiments, while Rice's (1987) analytical solution has four sectors. The 1-2 sector boundary angles are in close agreement for Orientation II and both the experiments and the analytical solution have a sector boundary near 90°, but the other sector boundaries observed in the experiments are not present in the analytical solution.

The experimentally determined sector boundary angles for both orientations are compared in Table 4. The sector boundary structure of Orientation II was very similar to that of Orientation I investigated by Shield (1996), however, there are several clear differences between Orientations I and II. The most notable difference is the additional sector observed in Orientation II results. Slip bands at 180° from the x_1 axis were observed in Sectors 2 and 3 in addition to the 55° and 125° slip bands already present. These slip bands suggested the presence of an additional sector boundary at 83–89° from the x_1 axis. This additional boundary near 90° was not observed by Shield (1996) or in additional Cu samples tested with Orientation I (Crone, 1998). There are also significant discrepancies between the other sector boundary angles of the two orientations.

Another issue is the 90° difference of the observed slip band angle in each sector for the two orientations. Orientations I and II are related by a 90° rotation about the x_3 axis and the slip plane traces on the surface of observation are also rotated by 90°. But at each corner of the yield surface, and therefore within each sector, there are two possible active slip systems. One of these seems to always be preferred within a particular sector of both orientations.

As Fig. 1 shows, there are two possible slip plane trace angles at each corner of the yield surface. It is interesting to note that there is a preference for one of these slip systems at sector boundaries. Slip bands associated with the same slip system display persistent strain localization in samples of both Orientations I and II. Additionally, unlike a slip band, kink-link shear does not appear as a strain localization. No persistent strain localization bands occurred at angles associated with kink-like shear perpendicular to the slip plane.

5. Comparison to numerical calculations

The existing numerical solutions can be categorized by those that agree with the Rice's (1987) perfectly plastic analytical solutions and solutions that agree more closely with the experimental results. The numerical models that agree with Rice's analytical solutions are based on small strain theory, whereas the models that agree most closely with the experiments include finite deformations within the theory. The numerical work of Rice et al. (1990) has the same sector boundary angles as Rice's analytical solution for Orientation II. As discussed previously, there is poor agreement between the experimental sector boundary angles and Rice's solutions.

The numerical work of Mohan et al. (1992) incorporated isotropic hardening and Cuitino and Ortiz (1996) incorporated a diagonal hardening model and finite deformations. These investigators produced numerical solutions for the stress fields about the notch which looked very different from those presented by other investigators. Table 2 compares their results to the perfectly plastic analytical solutions and the experiments discussed above. It is notable that the numerical solutions do not agree with the analytical solution presented for Orientations I and II. As with Rice's (1987) solution, Mohan et al. (1992) predict the same sector boundary angles for Orientations I and II. This is not supported by the experimental evidence. For Orientation I, the numerical solution of Mohan et al. agrees well with the experimental sector boundary angles with the exception of boundary 2-3. For Orientation II, the numerical solution of Mohan et al. only agrees with two of the three sector boundary angles observed in the experiments.

Cuitino and Ortiz (1996) performed finite element calculations on Orientation II. As Table 2 shows, the first two sector boundary angles are within 5° of the experimental measurements, but the agreement is worse for other sector boundaries. The shape of the progression around the yield surface calculated with the finite element model is compared to the experimental results in Fig. 9. Although correlation between the numerically calculated and experimentally measured in-plane strain components is not perfect, there is good agreement between the numerical yield surface and the strain results plotted in strain space. The shapes are similar and the progression is counterclockwise for both.

Cuitino and Ortiz (1996) raise questions about the plane strain assumption used in the analytical work and the reliance on surface strain measurements in the experimental research. Cuitino and Ortiz use two key points to support their argument that the problem cannot be considered plane strain: numerical results for the central plane differ from the exterior plane; and one slip system dominates in the pair on the surface which would create out of plane displacements.

The current experimental results can address both of these points. The difference between the numerical results for the central and exterior planes is most dramatically indicated by the presence of an additional sector in the interior plane with a boundary at 135° from the x_1 axis. For Orientation II, an additional sector is also observed in the experiments behind the notch tip at approximately 150° from the x_1 axis on the surface of the sample. The existence of an additional sector near the notch face in the new experimental observations agrees with the numerical results for the specimen interior thus it appears that the surface measurements do correlate with the interior calculations.

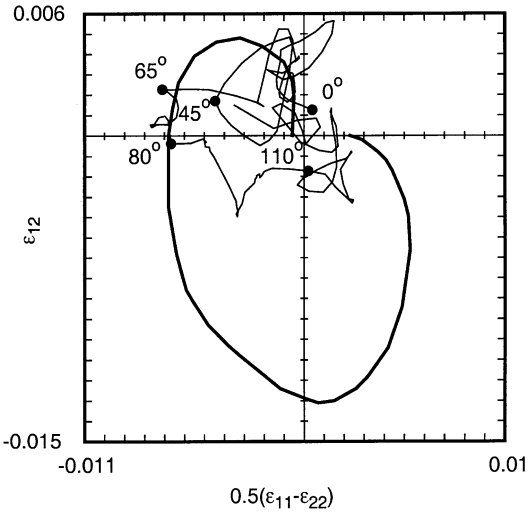

Fig. 9. The progression around the yield surface in Cuitino and Ortiz's (1996) numerical model is shown as a dark line overlayed on the experimental results in strain space for sample CB7 of Orientation II. The numerical calculations used a hardening exponent of $N = 2$.

The dominant slip system, discussed by Mohan et al. (1992) and Cuitino and Ortiz (1996), occurs in the numerical solutions at a small angle from the x_1 axis on a slip system oriented 90° from the x_1 axis. Optical observations show few slip lines in this area and virtually no out of plane tilt of the surface is detected with the DIC optical method. Some localized out of plane deformation is observed in small regions near the notch at angles greater than 90°.

Shield (1996) and Shield and Kim (1994) calculated that the in-plane volume change ($\varepsilon_{11} + \varepsilon_{22}$) was near zero for the two samples they tested. Assuming incompressible plastic flow, this measure indicated that the out-of-plane normal plastic strain, ε_{33}, was negligible and that the deformation could be considered to approximate plane strain conditions. The in-plane volume change was small for the CuBe results presented here with the exception of a few specific angles. For Orientation II, significant values of $\varepsilon_{11} + \varepsilon_{22}$ were observed between ± 80–95° from the x_1 axis particularly in the softer samples tested. The tilt observed at these angles with a DIC microscope further indicates that there is out-of-plane surface deformation in these regions near the notch tip. It is important to note that the nonzero $\varepsilon_{11} + \varepsilon_{22}$ values are away from the x_1 axis in contrast to the location noted in the numerical results of Cuitino and Ortiz (1996). The value of $\varepsilon_{11} + \varepsilon_{22}$ at small angles from the x_1 axis is negligible in the experiments.

6. Conclusion

Rice's (1987) solution for plastic deformation near a crack tip in an elastic-perfectly plastic single crystal forecasted the existence of constant stress sectors with sharp

boundaries. Although the general structure of the experimental results follows his analytical solution, the sector boundary angles predicted do not agree with the experiments. Because the analytical and numerical work assumes that the slip and kink directions are interchangeable, the solutions for Orientations I and II are the same. However, experimental results show that the sector boundary angles observed in copper single crystal samples differ between Orientation I investigated by Shield (1996) and Orientation II reported here. Additionally, differences in the sector boundary angles are observed between experimental results in BCC and FCC crystals. As discussed by Rice (1987) and shown by Zhang and Huang (1994), the analytical solution is not unique. Two additional three sector solutions were constructed by Zhang and Huang (1994) which satisfy the conditions posed by Rice (1987); although these solutions are not supported by the experimental findings either.

It has been shown experimentally that sector boundary angles do not exclusively correspond to directions of $\boldsymbol{S}$ and $\boldsymbol{N}$. In both Orientations I and II, sector boundary angles are observed which do not match angles at which slip and kink can occur in these crystallographic orientations. This finding is contrary to the assumption that all sector boundary angles occur in the direction of $\boldsymbol{S}$ or $\boldsymbol{N}$ in the fully plastic perfectly plastic analytical solution. It is also clear that the sectors observed are not 90° in extent and thus they do not correspond to the solutions proposed by Zhang and Huang (1994).

The experiments also lead one to conclude that some sectors in the deformation field remain elastic even after large amounts of deformation have occurred elsewhere. These sectors contain few or no persistent strain localization bands and have low measured strain levels. These elastic sectors have repercussions for analytical perfectly plastic solutions which have been presented in the literature. The assumption that the entire field around the crack tip is at yield must be revisited.

Results from the numerical models of Mohan et al. (1992) and Cuitino and Ortiz (1996) are somewhat more consistent with the experimental findings, in both the number of sectors and the angles of the sector boundaries. However, the three dimensional model of Cuitino and Ortiz predicts significant decay in strain with radius in all sectors and indistinct boundaries between sectors, conclusions that are not supported by the experimental observations. Cuitino and Ortiz also conclude from their numerical results that the problem is not plane strain, but this is contradicted by the data presented here. The angles at which the in-plane volume change is appreciable are not those predicted by the numerical results of Mohan et al. (1992). The central plane solution given by Cuitino and Ortiz (1996) is found to have fair correlation with experimental observation. These conclusions lend credibility to the comparison of measurements on the surface of a thick single crystal four-point-bend sample to plane strain theoretical results.

The research presented has further confirmed that the structure of the deformation field near a notch in a metallic single crystal is linked to crystallographic orientation. Although Rice (1987) captures the main features of the deformation experimentally observed near a notch in FCC copper and copper–beryllium single crystals, a more complex analytical solution is required to account for the sector boundary angles and the elastic sectors noted in these experiments. Research is currently underway to develop an analytical solution that more closely correlates with the experimental findings.

Acknowledgements

The authors acknowledge the support of the National Science Foundation (grant number MSS-9257945-2). WCC also gratefully acknowledges the support of a Dissertation Fellowship from the American Association of University Women and an Amelia Earhart Fellowship from Zonta International. Portions of this research were conducted in the University of Minnesota Center for Interfacial Engineering, University of Minnesota Microtechnology Laboratory, and the crystal growth facility of Prof. R.D. James.

References

Bastawros, A.F., Kim, K.-S., 1998. Experimental analysis of deformation induced microstructure near a crack tip in a hardened copper crystal. MRS Proceedings 539, 251–256.

Cho, J.W., Yu, J., 1991. Near-crack-tip deformation in copper single-crystals. Philosphical Magazine Letters 64 (4), 175–182.

Crone, W.C., Drugan, W.J., 2001. Comparison of experiment and theory for crack tip fields in ductile single crystals. International Congress of Fracture, ICF 10, Honolulu, HI.

Crone, W.C., 2000. Compositional variation and precipitate structures of copper beryllium single crystals grown by the Bridgman technique. Journal of Crystal Growth 218, 381–389.

Crone, W.C., 1998. Experimental investigation of the deformation near a notch tip in metallic single crystals. Ph.D. Thesis, University of Minnesota.

Cuitino, A.M., Ortiz, M., 1996. Three-dimensional crack-tip fields in four-point bending copper single-crystal specimens. Journal of the Mechanics and Physics of Solids 44 (6), 863–904.

Drugan, W.J., 2001. Asymptotic solutions for tensile crack tip fields without kink-type shear bands in elastic-ideally plastic single crystals. Journal of the Mechanics and Physics of Solids 49 (9), 2155–2176.

Mohan, R., Ortiz, M., Shih, C.F., 1992. An analysis of cracks in ductile single crystals—II. Mode I loading. Journal of the Mechanics and Physics of Solids 40 (2), 315–337.

Rice, J.R., Hawk, D.E., Asaro, R.J., 1990. Crack tip fields in ductile crystals. International Journal of Fracture 42, 301–321.

Rice, J.R., 1987. Tensile crack tip fields in elastic-ideally plastic crystals. Mechanics of Materials 6, 317–335.

Rice, J.R., 1973. Plane strain slip line theory for anisotropic rigid/plastic materials. Journal of the Mechanics and Physics of Solids 21, 63–74.

Saeedvafa, M., Rice, J.R., 1989. Crack tip singular fields in ductile crystals with taylor power-law hardening, II: plane strain. Journal of the Mechanics and Physics of Solids 37 (6), 673–691.

Shield, T.W., Kim, K.S., 1994. Experimental measurement of the near tip strain field in an iron–silicon single crystal. Journal of the Mechanics and Physics of Solids 42 (5), 845–873.

Shield, T.W., Kim, K.S., 1991. Diffraction theory of optical interference Moiré and a device for production of variable virtual reference gratings: a Moiré microscope. Experimental Mechanics 31 (2) 126–134.

Shield, T.W., 1996. An experimental study of the plastic strain fields near a notch tip in a copper single crystal during loading. Acta Materialia 44 (4), 1547–1561.

Tetelman, A.S., Robertson, W.D., 1963. Direct observation and analysis of crack propogation in iron-3% silicon single crystals. Acta Metallurgica 11 (5), 415–426.

Zhang, H.W., Huang, Y., 1994. Asymptotic tensile crack-tip stress fields in elastic-perfectly plastic crystals. International Journal of Fracture 67, 133–142.